Band-ratio or spectral-curvature algorithms for satellite remote sensing?

Zhongping Lee and Kendall L. Carder

For the retrieval of chlorophyll concentrations or the total absorption coefficients of oceanic waters based on water color, there are algorithms that use either band ratios or spectral curvatures of remote-sensing reflectance or water leaving radiance. We show that band-ratio algorithms have the potential to be applied to a wider dynamic range of oceanic waters, whereas spectral-curvature algorithms show stable performance as long as the data set falls within the appropriate range. © 2000 Optical Society of America

OCIS codes: 280.0280, 010.4450.

1. Introduction

For the retrieval of chlorophyll concentrations or the total absorption coefficient for oceanic waters based on water color, there are algorithms that use either band ratio[1–8] or spectral curvature[9,10] of remote-sensing reflectance or water-leaving radiance. Although band-ratio algorithms are popular and widely used, there are few comparisons about their performance, and the advantages and drawbacks of the two kinds of algorithm have not been clearly delineated. By comparing the sensitivity and performance of absorption algorithms using a two-band ratio and a spectral-curvature approach, we show that two-band-ratio algorithms remain sensitive over a wider dynamic range of absorption values and perform better at low- and high-absorption values.

To evaluate the sensitivity and performance of a two-band-ratio algorithm and a spectral-curvature algorithm to variations in the absorption coefficient, we created a data set including both case-1 and case-2 waters[3] by using a remote-sensing reflectance model for deep waters.[11] In this data set, we varied the pigment concentration C and other bio-optical parameters in a way that closely mimics the natural field. The following provides details of the data creation.

For homogeneous, optically deep waters, subsurface remote-sensing reflectance is a function of in-water absorption and scattering coefficients.[11–13] Generally,

$$r_{rs} \approx g(b_b/a), \tag{1}$$

where g is a weak function of b_b/a with a typical value[14] of approximately 0.09. a and b_b are the total absorption and backscattering coefficients, respectively, and,

$$\begin{aligned} a(\lambda) &= a_w(\lambda) + a_p(\lambda) + a_g(\lambda), \\ b_b(\lambda) &= b_{bw}(\lambda) + b_{bp}(\lambda), \end{aligned} \tag{2}$$

where a_w, a_p, and a_g are the absorption coefficients for water molecules, pigments, and gelbstoff–detritus, respectively, and b_{bw} and b_{bp} are the backscattering coefficients for water molecules and suspended particles. Values for a_w and b_{bw} are already known.[15,16] We used the following bio-optical models[12,13] to create optical data that simulates ocean waters:

$$\begin{aligned} a_p(440) &= 0.06C^{0.65}, \\ a_g(440) &= p_1{*}a_p(440), \\ b_{bp}(550) &= \{0.002 + 0.02[0.5 \\ &\quad - 0.25\log(C)]\}{*}p_2{*}C^{0.62}, \end{aligned} \tag{3}$$

Further,

$$\begin{aligned} a_p(\lambda) &= \{a_0(\lambda) + a_1(\lambda)\ln[a_p(440)]\}a_p(440), \\ b_{bp}(\lambda) &= b_{bp}(550)\left(\frac{550}{\lambda}\right)^n, \\ a_g(\lambda) &= a_g(440)\exp[-0.015(\lambda - 440)], \end{aligned} \tag{4}$$

The authors are with the Department of Marine Science, University of South Florida, St. Petersburg, Florida 33701. The e-mail address for Z. Lee is zplee@monty.marine.usf.edu.

Received 29 September 1999; revised manuscript received 12 April 2000.

0003-6935/00/244377-04$15.00/0

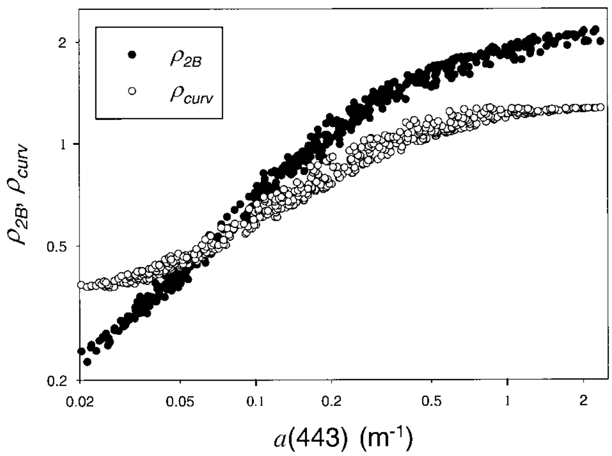

Fig. 1. Relationship between the total absorption coefficient at 443 nm and a two-band ratio and a spectral curvature of remote-sensing reflectance.

where values for $a_0(\lambda)$ and $a_1(\lambda)$ are known.[17] Note that C is used only as a free parameter for the designation of a wide range of absorption values.

For case-1 waters,[12,13] $p_1 \approx 0.8$, $p_2 \approx 0.3$, and $n \approx 1.0$, and all the optical parameters covary with C values. Since many natural waters are not case 1, we perturbed the case-1 parameters as follows:

$$p_1 = 0.5 + \frac{3.5\Re_1{}^* a_p(440)}{0.02 + a_p(440)},$$
$$p_2 = 0.1 + 0.5\Re_2,$$
$$n = 0.2 + \frac{1.5 + \Re_3}{1 + C}, \qquad (5)$$

where $\Re_1$, $\Re_2$, and $\Re_3$ are random values between 0 and 1. These kinds of perturbation result in p_1, p_2, and n random values for each C value, but fall within a range that is consistent with field observations.[12,13,18] For example, p_1 ranges between 0.5 and 4.0 in general, p_2 between 0.1 and 0.6, and n between 0.2 and 2.5. Also, to be consistent with field observations, the range for p_1 is narrower for low C values (open ocean), wider for high C values (coastal), and n decreases when C values increase, but in a random way for both p_1 and n.

Thus, for each C value, there is a range of simulated r_{rs} spectra that is not just a function of C, but is also a function of the random values of $\Re_1$, $\Re_2$, and $\Re_3$. For a C range of from 0.05 to 30 mg/m^3, 480 r_{rs} spectra were simulated.

We calculated the following ratio and curvature[10] values from the simulated data set:

$$\rho_{2B} = \frac{r_{rs}(555)}{r_{rs}(490)},$$
$$\rho_{curv} = \frac{r_{rs}(443)}{r_{rs}(490)} \bigg/ \frac{r_{rs}(490)}{r_{rs}(555)}. \qquad (6)$$

Figure 1 shows how ρ_{2B} and ρ_{curv} relate to $a(443)$. In the log–log coordinates between $a(443)$ and ρ_{2B} and ρ_{curv}, ρ_{2B} increases with $a(443)$ in a linear manner for $a(443)$ values less than 0.2 m^{-1}, and then increases at a reduced rate. ρ_{curv} approaches asymptotic values for both high and low $a(443)$ values. In terms of the dynamic range, for the entire $a(443)$ range (from ~0.02 to ~2.4 m^{-1}), ρ_{2B} falls within the range from ~0.23 to ~2.16, but ρ_{curv} ranges from ~0.37 to ~1.28, or half of the dynamic range of ρ_{2B}. For $a(443)$ greater than 0.4 m^{-1} (typical for near-shore coastal waters), ρ_{2B} varies from ~1.47 to ~2.16, whereas ρ_{curv} varies from ~1.07 to ~1.28, or one third of the dynamic range. For $a(443)$ less than 0.07 m^{-1} [equivalent to a pigment concentration of ~0.4 mg/m^3 for case-1 waters, and greater than 50% of the Sea-viewing Wide Field-of-view Sensor Bio-optical Algorithm Mini-workshop (SeaBAM) data[19] have a pigment concentration of less than 0.4 mg/m^3], ρ_{2B} varies from ~0.23 to ~0.54, whereas ρ_{curv} varies from ~0.38 to ~0.50, again a factor of 2 smaller. These results suggest that the 555–490 band ratio is more sensitive to $a(443)$ than the 555–490–443 curvature approach. In other words, because of the narrow range in ρ_{curv}, much more precise measurements of remote-sensing reflectance are required if ρ_{curv}-based algorithms are applied to coastal waters. This is consistent with the analysis of Campbell and Esaias[9] with regard to spectral-curvature algorithms for chlorophyll concentration.

The reduction in sensitivity of ρ_{curv} can be explained as follows. For a two-band r_{rs} ratio between 555 and 490,

$$\rho_{2B} = \frac{r_{rs}(555)}{r_{rs}(490)} = \frac{g(555)}{g(490)} \frac{b_b(555)}{b_b(490)} \frac{a(490)}{a(555)}. \qquad (7)$$

As g is only a weak function of wavelength for oceanic waters,[12,14]

$$\rho_{2B} \approx \frac{b_b(555)}{b_b(490)} \frac{a(490)}{a(555)} = \beta_{2B} \frac{a(490)}{a(555)}. \qquad (8)$$

Using a spectral curvature[9,10] among 443, 490, and 555 nm, we have

$$\rho_{curv} = \frac{r_{rs}(555)}{r_{rs}(490)} \bigg/ \frac{r_{rs}(490)}{r_{rs}(443)} \approx \frac{b_b(555)b_b(443)}{[b_b(490)]^2} \frac{[a(490)]^2}{a(555)a(443)} \qquad (9)$$

or

$$\rho_{curv} \approx \beta_{3B} \frac{a(490)}{a(443)} \bigg/ \frac{a(555)}{a(490)} = \beta_{3B}\alpha_{23}/\alpha_{12}, \qquad (10)$$

where β_{3B} is the three-band ratio of backscattering coefficient, α_{12} is the ratio of $a(555)/a(490)$, and α_{23} is the ratio of $a(490)/a(443)$.

For oceanic waters, the quantities of a or b_b can vary by orders of magnitude from place to place. As a and b_b are sums of in-water components,[4,12,14] all $a(\lambda)$ and $b_b(\lambda)$ values increase with an increase of in-water constituents, but at different rates for dif-

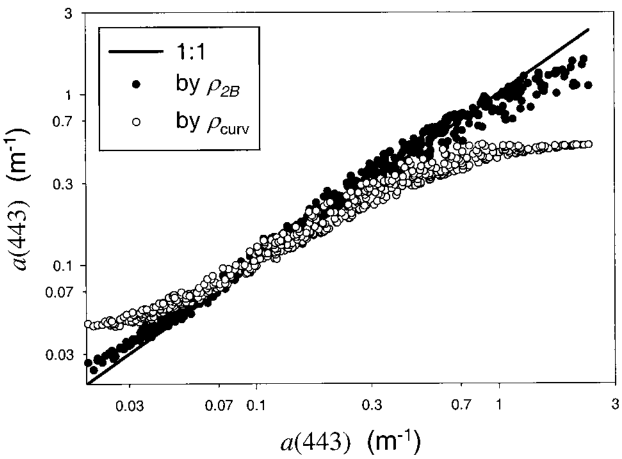

Fig. 2. Comparison of algorithm derived $a(443)$ versus real $a(443)$ values.

ferent wavelengths. Because of this feature, the ratio $a(555)/a(490)$ or $b_b(555)/b_b(490)$ is less sensitive than the individual $a(555)$ or $a(490)$ or $b_b(555)$ or $b_b(490)$ to the change of in-water constituents. In addition, a ratio of those ratios, e.g., α_{23}/α_{12}, further reduces this sensitivity, resulting in α_{23}/α_{12} that is more insensitive than $a(443)$, $a(490)$, or $a(555)$ to the change of in-water constituents.

To test the above analysis, we applied a band-ratio algorithm and a spectral-curvature algorithm to the above simulated case-2 data set. Both algorithms were independently developed based on specific field data sets. The band-ratio algorithm is a recent update of the Lee *et al.*[6] empirical algorithm with additional data. This updated algorithm is

$$a(443) = \exp\{-1.752 + 1.326\gamma + 0.118[\exp(\gamma)]^3\}, \quad (11)$$

where $\gamma = \ln[r_{rs}(555)/r_{rs}(490)]$.

Applying this two-band-ratio algorithm to the simulated data set, yields a root-mean-square error[6] (rmse) of approximately 13% for the entire $a(443)$ range (see Fig. 2). For three separate $a(443)$ ranges, rmse values are ~11% ($N = 137$) for $a(443)$ less than 0.07 m^{-1}, ~11% ($N = 193$) for $a(443)$ between 0.07 and 0.4 m^{-1}, and ~18% ($N = 150$) for $a(443)$ greater than 0.4 m^{-1}.

Applying the curvature algorithm of Barnard *et al.*,[10] yields a rmse value of approximately 43% for the entire $a(443)$ range. The rmse values are ~36% for $a(443)$ less than 0.07 m^{-1}, ~13% for $a(443)$ between 0.07 and 0.4 m^{-1}, and ~103% for $a(443)$ greater than 0.4 m^{-1}. It is clear from Fig. 2 that this curvature algorithm overestimates $a(443)$ for values less than 0.07 m^{-1}, and substantially underestimates $a(443)$ for values greater than 0.4 m^{-1}. However, this curvature algorithm works quite well for the middle range (0.07–0.4 m^{-1}), which is consistent with the results of Barnard *et al.*[10]

It is interesting that both algorithms performed similarly for the middle range, but the two-band-ratio algorithm performed better at both low- and high-absorption values. These results suggest that three or more curvature algorithms with different sets of wavelength bands could be useful for different ranges of total absorption coefficients. If one uses the two-band-ratio algorithm, another empirical algorithm might be required for $a(443)$ values greater than 1.0 m^{-1}, such as the switch method by Gordon *et al.*[20] for the Coastal Zone Color Scanner algorithm.

Financial support was provided by NASA through grants NAS5-97137 and NAS5-31716, Office of Naval Research through grant N00014-96-I-5013, and the National Oceanic and Atmospheric Administration Coastal Ocean Program R/NCOP-5.

References

1. D. K. Clark, E. T. Baker, and A. E. Strong, "Upwelled spectral radiance distribution in relation to particulate matter in sea water," Boundary-Layer Meteorol. **18,** 287–298 (1980).
2. R. W. Austin and T. J. Petzold, "The determination of the diffuse attenuation coefficient of sea water using the coastal zone color scanner," in *Oceanography from Space*, J. F. R. Gower, ed. (Plenum, New York, 1981), pp. 239–256.
3. A. Morel and L. Prieur, "Analysis of variations in ocean color," Limnol. Oceanogr. **22,** 709–722 (1977).
4. H. R. Gordon, D. K. Clark, J. W. Brown, O. B. Brown, R. H. Evans, and W. W. Broenkow, "Phytoplankton pigment concentrations in the Middle Atlantic Bight: comparison of ship determinations and CZCS estimates," Appl. Opt. **22,** 20–36 (1983).
5. J. Aiken, G. F. Moore, C. C. Trees, S. B. Hooker, and D. K. Clark, "The SeaWiFS CZCS-type pigment algorithm," SeaWiFS Technical Report Series, NASA Tech. Memo. 104566, 29 (NASA Goddard Space Flight Center, Greenbelt, Md., 1995).
6. Z. P. Lee, K. L. Carder, R. G. Steward, T. G. Peacock, C. O. Davis, and J. S. Patch, "An empirical algorithm for light absorption by ocean water based on color," J. Geophys. Res. **103,** 27967–27978 (1998).
7. J. E. O'Reilly, S. Maritorena, B. G. Mitchell, D. A. Siegel, K. L. Carder, S. A. Garver, M. Mahru, and C. McClain, "Ocean color chlorophyll algorithms for SeaWiFS," J. Geophys. Res. **103,** 24937–24953 (1998).
8. K. L. Carder, F. R. Chen, Z. P. Lee, S. K. Hawes, and D. Kamykowski, "Semianalytic moderate-resolution imaging spectrometer algorithms for chlorophyll *a* and absorption with bio-optical domains based on nitrate-depletion temperatures," J. Geophys. Res. **104,** 5403–5421 (1999).
9. J. W. Campbell and W. E. Esaias, "Basis for spectral curvature algorithms in remote sensing of chlorophyll," Appl. Opt. **22,** 1084–1093 (1983).
10. A. H. Barnard, J. R. Zaneveld, and W. S. Pegau, "*In situ* determination of the remotely sensed reflectance and the absorption coefficient: closure and inversion," Appl. Opt. **38,** 5108–5117 (1999).
11. Z. P. Lee, K. L. Carder, C. D. Mobley, R. G. Steward, and J. S. Patch, "Hyperspectral remote sensing for shallow waters: 2. Deriving bottom depths and water properties by optimization," Appl. Opt. **38,** 3831–3843 (1999).
12. H. R. Gordon, O. B. Brown, R. H. Evans, J. W. Brown, R. C. Smith, K. S. Baker, and D. K. Clark, "A semianalytic radiance model of ocean color," J. Geophys. Res. **93,** 10909–10924 (1988).
13. A. Morel, "Optical modeling of the upper ocean in relation to its biogenous matter content (case I waters)," J. Geophys. Res. **93,** 10749–10768 (1988).
14. A. Morel and B. Gentili, "Diffuse reflectance of oceanic waters. II. Bidirectional aspects," Appl. Opt. **32,** 6864–6879 (1993).

15. R. Pope, and E. Fry, “Absorption spectrum (380–700 nm) of pure water: II. Integrating cavity measurements,” Appl. Opt. **36,** 8710–8723 (1997).
16. A. Morel, “Optical properties of pure water and pure sea water,” in *Optical Aspects of Oceanography*, N. G. Jerlov and E. S. Nielsen, eds. (Academic, New York, 1974), pp. 1–24.
17. Z. P. Lee, K. L. Carder, C. D. Mobley, R. G. Steward, and J. S. Patch, “Hyperspectral remote sensing for shallow waters. 1. A semianalytical model,” Appl. Opt. **37,** 6329–6338 (1998).
18. S. Sathyendranath, L. Prieur, and A. Morel, “A three-component model of ocean colour and its application to remote sensing of phytoplankton pigments in coastal waters,” Int. J. Remote Sensing **10,** 1373–1394 (1989).
19. J. E. O'Reilly, S. Maritorena, B. G. Mitchell, D. A. Siegel, K. L. Carder, S. A. Garver, M. Mahru, and C. McClain, “Ocean color chlorophyll algorithms for SeaWiFS,” J. Geophy. Res. **103,** 24937–24953 (1998).
20. H. R. Gordon, D. K. Clark, J. W. Brown, O. B. Brown, R. H. Evans, and W. W. Broenkow, “Phytoplankton pigment concentration in the Middle Atlantic Bight: comparison of ship determinations and CZCS estimates,” Appl. Opt. **22,** 20–36 (1983).